Tribhuvan University

Institute of Engineering

Pulchowk Campus

B-08-BME-2019-2024

Design and Fabricate a Toroidal Turbine for Low Head Hydropower Application

by

Dipesh Dhamala(076BME010)

Mahesh Khadka(076BME019)

Milan Gurung(076BME021)

Shreedhar Poudel(076BME041)

A REPORT SUBMITTED TO THE DEPARTMENT OF MECHANICAL AND AEROSPACE ENGINEERING IN PARTIAL FULFILLMENT OF THE REQUIREMENT FOR THE DEGREE OF BACHELOR IN MECHANICAL ENGINEERING

DEPARTMENT OF MECHANICAL AND AEROSPACE ENGINEERINGLALITPUR, NEPAL

May, 2024

Copyright

TRIBHUVAN UNIVERSITY

INSTITUTE OF ENGINEERING

PULCHOWK CAMPUS

DEPARTMENT OF MECHANICAL AND AEROSPACE ENGINEERING

The undersigned certify that they have read, and recommended to the Institute of Engineering for acceptance, a project report entitled "Design and fabricate a toroidal turbine for low head application," submitted by Dipesh Dhamala, Mahesh Khadka, Milan Gurung, Shreedhar Poudel in partial fulfillment of the requirements for the degree of Bachelor of Mechanical Engineering.

Supervisor, Tek Raj Subedi

Assistant Professor

Department of Mechanical and Aerospace Engineering

External Examiner, Assistant Prof. Raj Kumar Chaulagai

Department of Automobile and Mechanical Engineering

Thapathali Campus

Committee Chairperson, Asst. Prof. Dr. Sudip Bhattarai

Head of Department

Department of Mechanical and Aerospace Engineering

10th April 2024

Date

ABSTRACT

This final year project investigates the design, modeling, simulation, fabrication, and experimental testing of a toroidal turbine for low head hydropower applications. Toroidal turbines are a novel and innovative technology that shows promise for hydropower generation, especially in low head situations. The project aims to enhance the understanding of toroidal turbine geometry and efficiency through advanced computational fluid dynamics (CFD) simulations and experimental validation. Initially, limited data and information posed challenges, but insights from studies by other engineers and available research papers provided a foundation for turbine development. Recent advancements in manufacturing processes have made the production of this complex geometry more viable.

The project mathematically defines the toroidal turbine geometry and develops a three-dimensional model using CAD software. ANSYS Fluent is employed for CFD simulations to analyze flow behavior, pressure distribution, and the designed turbine's efficiency under specified operating conditions. The simulations predict an efficiency of 58.7% for the designed toroidal turbine. A miniature physical model of the turbine is fabricated using 3D printing and investment casting processes. An experimental setup configuration is constructed to test the fabricated turbine model. During experimental testing, the turbine is connected to a dynamo, and its electrical output is measured. The experimental results show a rotational speed of 320 rev/min and an overall system efficiency of 17.41%. The project highlights the potential of toroidal turbines for hydropower applications while identifying areas for further improvement and optimization in design, simulation, fabrication, and experimental testing methodologies.

ACKNOWLEDGEMENT

We extend our heartfelt gratitude to all those who contributed to the toroidal turbines project. Our sincere appreciation goes to our esteemed project supervisor, Asst. Prof. Tek Raj Subedi, and the Department of Mechanical and Aerospace Engineering at the Institute of Engineering, Pulchowk Campus, for their invaluable support and collaborative efforts throughout this endeavor. We are deeply thankful to our project supervisor for their unwavering guidance, insightful feedback, and continuous encouragement, which significantly enriched the research process and contributed to the project's success.

Our deepest acknowledgment goes to Mr. Nitesh Tuladhar for his invaluable assistance, recommendations, and expertise in the fabrication and casting of the turbine. Additionally, we express our gratitude to Mr. Sadan Shah for his skilled craftsmanship in fabricating the shaft. We also appreciate the Department of Mechanical Engineering for providing us with the opportunity and the Incubation and Innovation Center, where we conducted our fabrication and experimental work in a conducive environment.

Finally, we would like to extend our heartfelt thanks to all our respective teachers, staff, colleagues, and everyone who contributed in any way to this project. Their support, guidance, and encouragement were instrumental in our journey and the successful completion of this endeavor.

TABLE OF CONTENTS

LIST OF FIGURES

LIST OF TABLES

LIST OF ACRONYMS AND ABBREVIATIONS

3D	Three-Dimensional
BSL	Baseline
CAD	Computer-Aided Design
CFD	Computational Fluid Dynamics
CLT	Contracted and Loaded Tip
DC	Direct Current
KW	Kilo Watts
MW	Mega Watts
NACA	National Advisory Committee for Aeronautics
PLA	Polylactic Acid
RANS	Reynolds-averaged Navier-Stokes
SST	Shear Stress Transport

CHAPTER ONE: INTRODUCTION

1.1. Background

Hydropower is a sustainable energy source that harnesses the power of moving water to produce electricity. It is one of the earliest forms of renewable energy, utilized for centuries. The primary premise is to transform the kinetic energy of flowing or falling water into mechanical energy, which is then used to drive generators and generate electrical power. Hydropower plants use turbines that spin due to the force of moving water, and these turbines are coupled to generators that produce energy. The potential for power generation is determined by two fundamental factors: the height of water (head) and the volume of water flow. In comparison to fossil fuel-based power-generating technologies, hydropower provides a clean and sustainable alternative to meet electricity demand while reducing environmental impacts.

Hydropower plays a significant role in Nepal's energy landscape, capitalizing on the country's abundant water resources and topographical advantages. With an estimated hydropower potential of 83,000 MW (42,000 MW feasible), Nepal stands as one of the richest countries in terms of hydropower resources globally. In contrast, head plants with the dam and reservoir low-head hydropower projects tend to be more resilient to climate change, relying on continuous water flow rather than stored water, making them a reliable and sustainable energy option. The scales of hydropower schemes cover a broad range and are generally classified by power output. Depending on the capacities, hydropower projects are categorized as given in Table 1. Depending on the head, small hydropower plants may be further classified as low head (below 3 meters), medium head (from 30-75 meters), and high head (above 75 meters).[1]

Table 1: Classification of hydro plants based on power output [1]

Classification	Power Output
Small	2MW to 25 MW
Mini	100kW to 2 MW
micro	5kW to 100kW
Pico	< =5kW

A turbine is a mechanical device that converts the energy of a fluid, such as water, steam, or gas, into rotational motion. The working principle of a hydropower turbine is based on the conversion of the potential head and kinetic head into rotational mechanical energy. Water is directed onto the turbine blades, causing them to rotate. The rotation is transferred through a shaft, which connects the turbine to a generator, converting the mechanical energy into electrical energy. Hydropower turbines face specific challenges in terms of design, efficiency, and environmental considerations. Designing turbines that can handle variable flow rates, minimize cavitation, and reduce wear and tear on components is crucial. There are two main types of hydropower turbines: reaction and impulse.

Impulse Turbine: The impulse turbine converts the potential energy of the water to the mechanical energy of the rotor by the impact of water on the turbine blade. Moreover, the impulse generated by the force of water is reasonable for transferring the energy. The force of water on the buckets turns the wheel which powers generators. The Pelton Wheel is an example of an impulse turbine.

Reaction turbines are turbines that use the pressure as well as the velocity of the moving water to rotate. In a reaction turbine, a part of the head (H) acting on the turbine is converted into kinetic energy and the rest remains as the pressure head. Reaction turbine works based on the lift force generated on the impeller blades due to the difference of pressure between these two sets of blades which is called 'reaction pressure' because of its airfoil shape. The two main factors that determine the efficiency of a reaction turbine are the angle of attack of water and the profile of the runner blade. Guide vanes are provided to make sure water always hits blades with the optimum angle of attack. The most common types of reaction turbines are Propeller, Kaplan, and Francis.

A propellor turbine is an axial flow reaction turbine with fixed blades, well-suited for low-head, high-flow installations. The various components of the propellor turbine are shown in Figure 1. In a propeller, water enters the turbine laterally, gets deflected by the guide vanes, and then flows through the propeller subsequently flowing through the fixed airfoil-shaped blades, the propeller turbine typically features four to ten blades. The propeller turbine is a reaction turbine used for heads between 1m to 40m. [1]

[2]By the application of Bernoulli's equation to the inlet and outlet section of the runner blade,

$$\frac{p_1 - p_2}{\rho g} = W_{net} - \frac{V_1^2 - V_2^2}{2g}$$

Where p_1, p_2 = pressure at inlet and outlet

V_1, V_2 = absolute velocity at Inlet and outlet section

W_{net} = work done by the turbine runner

The head of the hydropower project and the flow rate available provide the necessary information for the turbine selection. Usually, for low-head and high-flow rate applications propeller turbine is used. A detailed analysis of the flow over time will need to be performed to choose a turbine that is best suited for a site. The diagram below shows the turbine selection criteria based on head and flow rate.

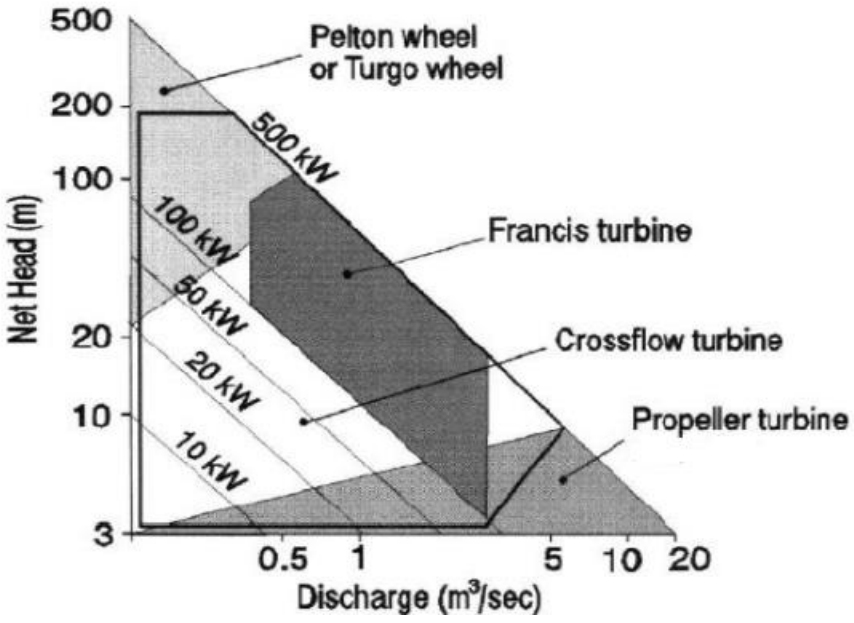

Figure 1: Turbine selection chart. [3]

[4] There are a lot of turbines for low-head applications for hydropower generation such as Archimedes Screw Turbines, Cross Flow Turbine, Gravitation Water Vortex Power Plant, The Power Pal Propeller Turbines, Hydrovolts Flipwing Turbines,

Gorlov Helical Turbines, Torcado Turbines, Niade Hydro Turbine, etc. Among these various turbines, Toroidal turbines are a relatively new type of turbine that uses a donut-shaped rotor and a stator to convert fluid or gas energy into rotational energy. Various other applications of toroidal shape have already been implemented in different propellors in drone and boat propellors and they have shown a significant increase in efficiency and reduced sound and vibration.

Toroidal turbines, though in early development, show promise for transforming renewable energy. Advances in manufacturing technology and ongoing research efforts address previous challenges, making these turbines more cost-effective. Limited data has been a hurdle, but studies, including those by the National Renewable Energy Laboratory and the University of Edinburgh, indicate toroidal turbines' potential efficiency advantages, particularly in low wind speeds and turbulent flows. Sharrow Marine's success with toroidal propellers further supports their viability. The project aims to evaluate toroidal turbine efficiency through advanced computational fluid dynamics simulations, building on positive outcomes seen in other sectors. The feasibility of toroidal turbines as a renewable energy solution depends on manufacturing costs versus efficiency gains, with ongoing research shaping the understanding of their potential impact.

1.2. Problem Statement

Toroidal turbines are a relatively new emerging technology with the potential to significantly improve the efficiency of fluid power conversion in a variety of applications, such as hydropower, wind power, and marine propulsion. These turbines offer the advantage of significantly improving efficiency compared to traditional designs. However, despite their promising potential, several challenges must be overcome for their widespread adoption. One of the main challenges in the development of toroidal turbines is their complex geometry, which poses difficulties in accurately modeling and analyzing the fluid dynamics involved. The unique shape and flow characteristics of the toroidal turbine require advanced computational fluid dynamics (CFD) simulations and experimental validation to understand and optimize its performance. Factors such as the number of blades, blade shape, and aspect ratio need to be carefully considered and tailored to different operating conditions. Finding the

optimal configuration that maximizes power output while minimizing losses and ensuring structural integrity is a critical aspect of toroidal turbine design.

1.3 Objectives

1.3.1 Main Objectives

The main objective is to design a toroidal turbine blade for low-head hydropower application with CFD simulation validated by experimental setup.

1.3.2 Specific Objectives

-To design a toroidal turbine for low-head application,

- Validation of the blade design using CFD analysis and simulation,

-To fabricate the blade profile and set up a miniature model of the experiment,

-To validate the computational data with the experimental values.

CHAPTER TWO: LITERATURE REVIEW

2.1. Blade Element Theory

Blade element theory involves breaking down the blade into numerous small sections, as depicted in Figure 2. Each of these sections can be viewed as an airfoil affected by a combined incident velocity W. This velocity comprises both an axial velocity V and a rotational velocity r, which changes gradually along the blade. Under typical operational circumstances, the advance angle β is smaller than the blade pitch angle θ at the section, resulting in the section having an angle of incidence α.

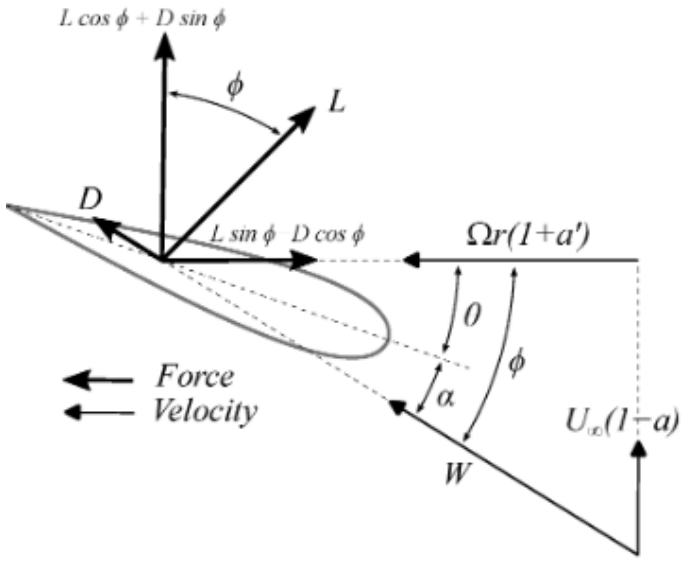

Figure 2: Blade element theory [5]

Thus the section will experience lift and drag forces on the blade profile. thus, the relation between elemental thrust and torques is given by

$$dT = \frac{1}{2}\rho Z v W^2 (c_l cos\theta - c_d sin\theta) dr$$

$$dQ = \frac{1}{2}\rho Z v W^2 (c_l sin\theta - c_d cos\theta) dr$$

where Z and c are the number of blades and the chord length of the section respectively.[5]

2.2. Propeller Lift Line Theory

The propeller lift line theory is a concept that describes the distribution of lift along the span of the propeller blade. It acknowledges that the lift distribution varies along the length of the blade. In the lifting line theory, the blades of the propeller are treated as a straight line. The lift-related circulation around the blade is replaced by a vortex filament. This vortex filament extends along a straight line.

The theory of the lifting line can be summarized as follows: the integration of the lifting force in the direction perpendicular to the current flowing into the propeller blade, the different pressure variations on the ridge, and the face of the propeller chord profile along the propeller profile chord.

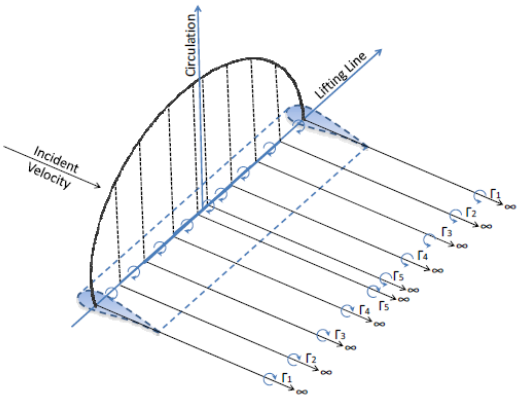

Figure 3: Vortex Pattern Representing a Lifting Blade [6]

The formula for a propeller of length c and width dx:

$$\mathrm{dL} = \mathrm{dx} \int_0^c \Delta p.\, dy = \rho V dx \int_0^c \Delta v.\, dy$$

The integral in equation (1.1) refers to the definition of vortex in fluid mechanics.

$$\int_0^c \Delta v.\, dy = \int v\, ds = \Gamma$$

Γ defines the vortex intensity. If we rewrite equation (1.1)

$$dL = \rho . v . \Gamma . \mathrm{dx}$$

We obtain the equation that gives the lift of the profile, known as the Kutta-Joukowsky theorem. According to this equation, the vortex intensity Γ must be known to find the lift of the profiles. [6]

2.3. Aerofoil Theory

An aerofoil, also known as an airfoil, is a specially shaped structure designed to maximize the efficiency of lifting forces while minimizing drag. Lift acts perpendicular to the motion, while drag is parallel to it. This principle is also applied to hydrofoils, which operate in water. The design of an aerofoil is based on Bernoulli's theorem, stating that the total pressure equals the sum of static pressure (from the weight of the air above) and dynamic pressure (due to air motion). As air flows over the curved upper surface of an aerofoil, its velocity increases, creating dynamic pressure and resulting in a pressure difference, known as lift, between the upper and lower surfaces due to the decrease in static pressure.

The initial NACA airfoil series was developed using mathematical equations to define both the curvature (camber) of the mean line (central line) and the thickness distribution along the length of the airfoil. This led to the creation of the NACA Four-Digit Series, the first set of airfoils designed using this approach. In this series, the first digit indicates the maximum camber (as a percentage of the chord, the length of the airfoil), the second digit specifies the location of the maximum camber (in tenths of the chord), and the last two digits represent the maximum thickness of the airfoil (as a percentage of the chord).

According to [7] the final coordinates for the airfoil's upper surface (xU, yU) and lower surface (xL, yL) using the following relationships.

$$x_U = x - y_t \sin\theta$$

$$y_U = y_c + y_y \cos\theta$$

$$x_L = x + y_t \sin\theta$$

$$y_L = y_c - y_y \cos\theta$$

where $\theta = \arctan\frac{dy_c}{dx}$

$$\pm y_t = \frac{t}{0.2}(0.2969\sqrt{x} - 0.126x - 0.3516x^2 + 0.2843x^3 - 0.1015x^4$$

2.4. Free Vortex Theory

The free vortex theory is a fundamental concept in fluid mechanics used to describe the behavior of vortices in an ideal, inviscid fluid. Vortices are regions of swirling or rotating motion within a fluid flow, characterized by fluid particles circulating around a central axis. The key assumptions include axisymmetric, irrotational, steady flow, and inviscid fluid. The velocity of the fluid is inversely proportional to the distance from the center.

Vortices are regions of swirling or rotating motion within a fluid flow, characterized by fluid particles circulating around a central axis. The velocity of the fluid (v) at a radial distance (r) from the center of rotation is given by the equation:

$$V * r = constant$$

The free vortex theory is crucial in axial flow turbines. It provides a theoretical foundation for understanding fluid flow dynamics within turbines, which aids in optimizing blade design and overall performance. This theory helps to build efficient turbines that extract the most energy from fluid flows by describing how fluid velocity varies with radial distance and emphasizing angular momentum conservation.

2.5. Axial Flow Turbine

Axial turbines are rotary machines designed to convert the energy from fluid flow into useful work. The axial turbine stage typically consists of a series of fixed guide vanes followed by a row of moving blades. When fluid enters the stator of the turbine, it does so with an absolute velocity v_1 at an angle α_1 relative to the axial (x) direction. As the fluid passes through the stator, it accelerates and exits with an absolute velocity v_2 at

an angle α_2. In the context of axial turbines, a key parameter is the rotor inlet relative velocity V_{r1} at an angle α_2. This velocity is determined vectorially by subtracting the blade speed U (tangential velocity of the rotor blades) from the absolute velocity v_2. The velocity triangle or diagram associated with axial turbines illustrates the relationships between these velocities and angles. This analysis is crucial for understanding the fluid dynamics and performance characteristics of axial turbines, aiding in the optimization of turbine design and efficiency for various applications in power generation and propulsion [8].

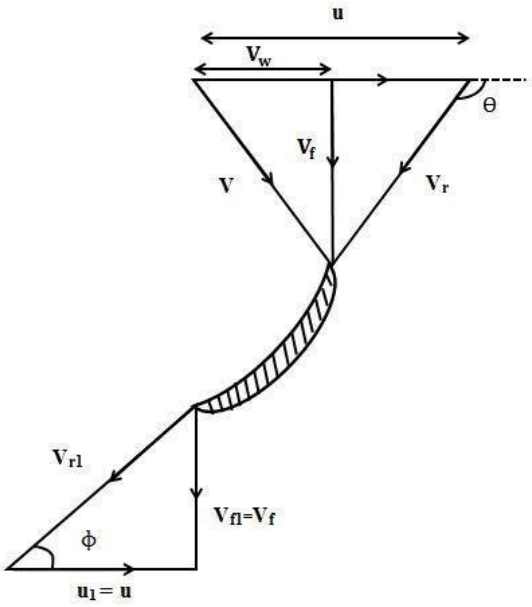

Figure 4: Velocity of axial flow turbine [8]

2.6. Eulers's Turbine Equation

Euler's turbine equation provides a general understanding of the work performed by the flowing fluid to generate power in a turbine. The tangential component of fluid velocity varies at the turbine's inlet and exit. The change in tangential velocity creates a change in angular momentum, which provides torque (τ), which generates power for the turbine. The equation is based on the conservation of angular momentum and energy.

The graphic shows the rotor of a generalized turbomachine with an angular velocity ω and a rotational axis 0-0. The fluid enters the rotor at radius r_1 with absolute velocity

V_1 and exits at radius r_2 with absolute velocity V_2.

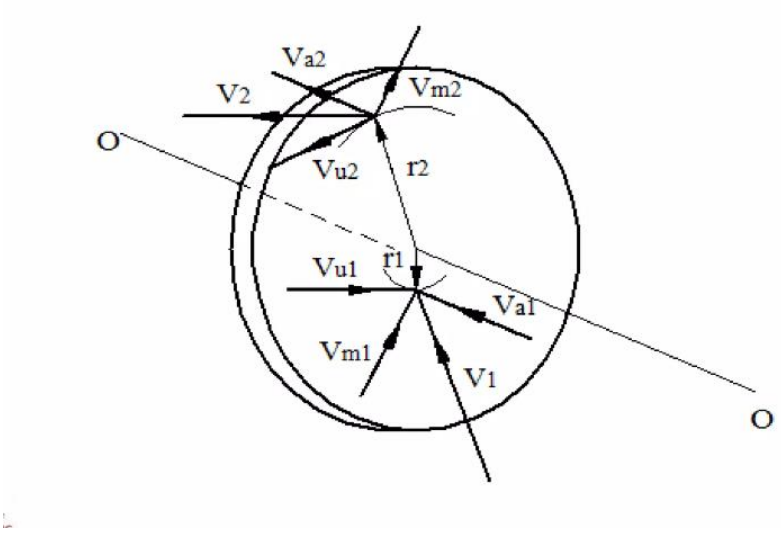

Figure 5: Fluid flow through a turbine [8]

Torque can be calculated by multiplying the mass flow rate, represented by $\dot{m}$ with the variation in the product of radius "r" and circumferential fluid velocity C_θ at both the inlet and outlet locations of the control volume encompassing the blade row. In the case of turbines, it's typically assumed that there is a constant mass flow rate.

$$\tau = \dot{m} * (r_2 V_{u2} - r_1 V_{u1})$$

The rate of work transferred from the fluid to the runner, $\dot{E}_t$ is the product of torque and angular velocity,ω.

$$\dot{E}_t = \tau * \omega = \dot{m} * (r_2 V_{u2} - r_1 V_{u1}) * \omega$$

2.7. Toroidal Geometry

The toroidal propeller comprises blades and a hub, with each blade forming a closed toroidal structure: a front section, a transition segment, and a rear section (Figure 4). The transition section smoothly connects the front and rear, allowing the blade's seamless transition. Although the blade lacks clear segment boundaries, its positions can be approximated by observing the skew angle distribution along the axis. The skew

angle gradually increases in the front and rear sections, while the transition section sees a rapid increase [9]. The root of the front section connects to the hub with a 0° skew angle, and the rear section's root has a 180° skew angle. Setting these angles ensures the blade profile points align on a common-radius coaxial cylindrical surface. The transition segment's profile, with a radius of R, is known as the tip, featuring an approximately 90° skew angle. Observing the geometric features of the toroidal propeller reveals its integration of the advantages of contra-rotating propellers and CLT (contracted and loaded tip) propellers.[10]

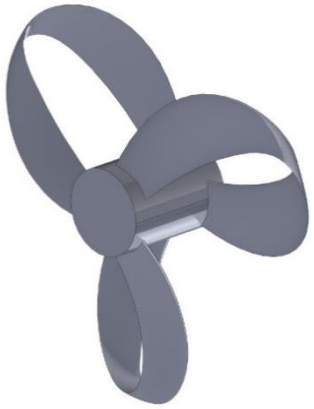

Figure 6: Toroidal propellor

Observing the geometric features of the toroidal propeller reveals its integration of the advantages of contra-rotating propellers and CLT (contracted and loaded tip) propellers. Contra-rotating propellers are a type of propulsor where two conventional propellers are mounted on the same tail shaft, rotating in the same direction. There's a certain distance between the fore and back propellers, causing the back propeller to operate within the wake of the fore propeller, leading to increased efficiency of the propeller. CLT propellers, known as tip-loaded propellers, are propellers equipped with endplates at the blade tips. These endplates are usually bent forward or backward, aiming to significantly reduce the shedding of vortices at the blade tips, thereby notably decreasing ship noise and vibrational forces, and enhancing propulsion efficiency [11].

2.8. Mathematical Expression of the Geometric Shape for Convection Propeller

There are various sources and references available [13] regarding the geometric parameters and mathematical expressions of the geometric shape of conventional propellers. The geometric design parameters of a conventional propeller include chord length, pitch, rake, and skew, as well as the curvature and thickness of the blade section airfoil. Assuming the propeller rotates in place, a rotating coordinate system fixed to the propeller is defined. The x-axis coincides with the propeller axis, with downstream considered positive; r represents the radial coordinate, considered positive outward; θ represents the angular coordinate, following the right-hand rule around the x-axis, as depicted in Figure 5. [12].

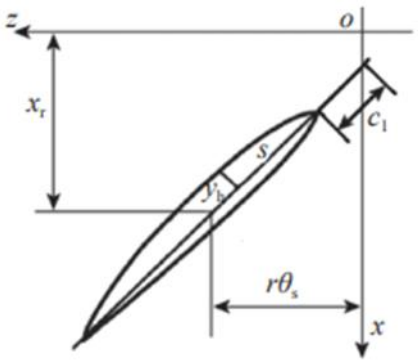

Figure 7: Expression of the standard propeller blade profile.

Considering the skew shape of the propeller blade which is represented by the skew angle, then each point on the blade section at a radius r in cylindrical coordinates can be expressed as:

$$x = x_T + \left(-\frac{b}{2} + s\right) sin\,\beta - \begin{bmatrix} y_b \\ y_f \end{bmatrix} cos\beta$$

$$r = r$$

$$\theta = \theta_s + \frac{1}{r}\left\{\left(-\frac{b}{2} + s\right) cos\,\beta + \begin{bmatrix} y_b \\ y_f \end{bmatrix} sin\beta\right\}$$

Where,

b = chord length of the blade section;

θ_s= skew angle;

β = total longitudinal inclination value;

x_T= blade surface reference line;

s = chordwise distance from the point on the blade section to the trailing edge;

y_b = distances from points on the back of the blade section to the chord line and

y_f = distances from points on the face of the blade section to the chord line.

In the Cartesian coordinate system o-XYZ, the coordinates of points can be expressed as:

$$x = x_T + \left(-\frac{b}{2} + s\right) sin\,\beta - \begin{bmatrix} y_b \\ y_f \end{bmatrix} cos\beta$$

$$y=r\cos\theta$$

$$z=r\sin\theta$$

2.9. Overview of ANSYS Fluent

ANSYS Fluent is a powerful computational fluid dynamics (CFD) software widely used for simulating fluid flow and heat transfer in engineering. It supports steady-state and transient simulations, handling both incompressible and compressible flows, laminar and turbulent flows, as well as multiphase flows and chemical reactions. The software offers advanced turbulence models and diverse heat transfer models including conduction, convection, and radiation. It finds applications across automotive, aerospace, chemical, energy, and biomedical engineering sectors. ANSYS fluent solves the equation of continuity and momentum using the finite volume method to obtain the results. The equation for conservation of mass, or continuity equation, can be written as follows[15]: -

$$\frac{\partial \rho}{\partial t} + \nabla \cdot (\rho \vec{v}) = S_m$$

Similarly, the conservation of momentum is described by: -

$$\frac{\partial}{\partial t}(\rho\vec{v}) + \nabla.(\rho\vec{v}\vec{v}) = -\nabla p.(\bar{\bar{\tau}}) + \rho\vec{g} + \vec{F}$$

Where p is the static pressure, $\bar{\bar{\tau}}$ is the stress tensor, and $\rho\vec{g}$ and $\overrightarrow{F}$ are the gravitational body force and external body forces respectively [15].

The stress tensor is given by: -

$$\bar{\bar{\tau}} = \mu[(\nabla\vec{v} + \nabla\vec{v}^T) - \frac{2}{3}\nabla.\vec{v}I$$

where μ is the molecular viscosity, $\bar{\bar{\tau}}$ is the unit tensor and the second term on the right-hand side is the effect of volume dilation [15].

2.10. Reynolds Averaging Turbulence Modeling

In Reynolds averaging, the solution variables in the instantaneous Navier-Stokes equations are decomposed into the mean and fluctuating components. For the velocity components:

$$u_i = \bar{u}_i + u_i'$$

Where $u_i$and $\bar{u}_i$ are the mean and fluctuating velocity components (i=1,2,3).

Likewise, for pressure and other scalar quantities:

$$\varphi = \bar{\varphi} + \varphi'$$

Where φ denotes a scalar such as pressure, energy, or species concentration.

When we replace flow variable expressions like this into the instantaneous continuity and momentum equations, then average them over time (with the overbar removed from the mean velocity), we obtain the time-averaged momentum equations, which can be represented in Cartesian tensor form as:

$$\frac{\partial \rho}{\partial t} + \frac{\partial}{\partial x_i}(\rho u_i) = 0$$

$$\frac{\partial}{\partial t}(\rho u_i) + \frac{\partial}{\partial x_j}(\rho u_i u_j) = -\frac{\partial \rho}{\partial x_i} + \frac{\partial}{\partial x_j} * [\mu(\frac{\partial u_i}{\partial x_j} + \frac{\partial u_j}{\partial x_i} - \frac{2}{3}\delta_{ij}\frac{\partial u_l}{\partial x_l} + \frac{\partial}{\partial x_j}(-\rho\overline{u_i' u_j'}))]$$

The above equations are called Reynolds-averaged Navier-Stokes (RANS) equations. They have the same general form as the instantaneous Navier-Stokes equations, with the velocities and other solution variables now representing time-averaged values [16].

2.11. Shear-Stress Transport (SST) k-ω Model

Shear-Stress Transport (SST) k-ω turbulence model is intended to precisely forecast turbulent flow characteristics, especially in intricate flow conditions such as boundary layer separation and unfavorable pressure gradients. The k-ω (k-omega) and k-ε (k-epsilon) turbulence models are combined in this model to overcome their respective shortcomings and improve overall performance.

The transport equations for turbulent kinetic energy (k) and specific dissipation rate (ω), which are essential for describing turbulence properties in various flow zones, are among the governing equations of the SST k-ω model. The following is how these equations are expressed:

$$\frac{\partial}{\partial t}(\rho k) + \frac{\partial}{\partial x_i}(\rho k u_i) = \frac{\partial}{\partial x_j}\left(\Gamma_k \frac{\partial k}{\partial x_j}\right) + G_k - Y_k + S_k + G_b$$

$$\frac{\partial}{\partial t}(\rho \omega) + \frac{\partial}{\partial x_i}(\rho \omega u_i) = \frac{\partial}{\partial x_j}\left(\Gamma_\omega \frac{\partial \omega}{\partial x_j}\right) + G_\omega - Y_\omega + S_\omega + G_{\omega b}$$

The equations involve terms for the generation of turbulence kinetic energy (Gk) and turbulence frequency (Gω) due to mean velocity gradients. Γk and Γω represent the effective diffusivities of k and ω. Yk and Yω account for the dissipation of k and ω due to turbulence. Sk and Sω are user-defined source terms. Gb and Gωb consider the effects of buoyancy on turbulence.

This function improves the model's ability to capture boundary layer effects, making it suitable for a wide range of flow conditions [16].

2.11. Scaling laws

Based on [18], Scaling laws for turbines are critical for forecasting the performance of scaled models based on prototype data. These rules allow us to understand how changes in size, speed, or other characteristics affect turbine performance without having to physically test each configuration. Scaling laws for turbines frequently use the Reynolds number to assure flow comparability between prototype and model turbines. The purpose of utilizing the Reynolds number in scaling laws is to ensure identical flow properties (such as turbulence levels, boundary layer behavior, and separation patterns) across different-sized turbines. Turbine scaling laws depend on flow rate (Q), head (H), power (P), and geometric and operational characteristics such as viscosity (μ), density (ρ), and modulus (κ). Using dimensional analysis, non-dimensional groups can be derived, such as:

$$\frac{P}{\rho\omega^3 D^5} = f\left[\frac{Q}{\omega D^3}, \frac{gH}{\omega^2 D^2}, \frac{\rho\omega D^2}{\mu}, \frac{\rho\omega^2 D^2}{\kappa}\right]$$

Where, $\frac{P}{\rho\omega^3 D^5}$ is power coefficient

$\frac{Q}{\omega D^3}$ is flow coefficient

$\frac{gH}{\omega^2 D^2}$ is head coefficient

$\frac{\rho\omega D^2}{\mu}$ Reynolds number based on a typical machine design

$\frac{\rho\omega^2 D^2}{\kappa}$ form of Mach number

The first three groups (Cp, φ, ψ) can be used to predict the dynamically similar performance of machines within the same family using scaling laws. Further, the scaling laws can be arranged in various forms, as shown in [18].

$$\frac{\mathbf{Q_p}}{\mathbf{Q_m}} = \left(\frac{\mathbf{H_p}}{\mathbf{H_m}}\right)^{1/2} * \left(\frac{\mathbf{D_P}}{\mathbf{D_m}}\right)^{2}$$

$$\frac{\mathbf{N_p}}{\mathbf{N_m}} = \left(\frac{\mathbf{H_p}}{\mathbf{H_m}}\right)^{1/2} * \left(\frac{\mathbf{D_P}}{\mathbf{D_m}}\right)^{-1}$$

$$\frac{\mathbf{P_p}}{\mathbf{P_m}} = \left(\frac{\mathbf{H_p}}{\mathbf{H_m}}\right)^{3/2} * \left(\frac{\mathbf{D_P}}{\mathbf{D_m}}\right)^{2}$$

2.13. Investment Casting

Investment casting is a casting process in which a wax pattern is used to form a disposable ceramic mold. The exact shape of the object to be cast is captured in a wax pattern then the same pattern is coated with a ceramic substance to form a ceramic mold. The mold is filled with molten metal, which is then allowed to cool. After that, the metal casting is broken out of the used mold.

The process begins with the creation of a precise metal die or mold, which takes into account the expected shrinkage of both the wax pattern and the ceramic material used in the casting process. This die serves as the foundation for creating multiple wax patterns, each meticulously crafted to replicate the desired shape of the final metal part. These wax patterns are formed by pouring molten wax over the metal die and allowing it to solidify. Once the wax patterns are ready, they are coated with a ceramic substance to form the mold. This ceramic mold, together with a gating system comprising sprues, runners, and risers, provides the framework for pouring the molten metal. During pouring, the molten metal is carefully introduced into the mold cavity through the gating system. The pre-heated mold allows for smooth metal flow, ensuring uniform distribution within the mold and preserving the intricate details of the wax pattern. After pouring, the metal is left to cool and solidify within the mold. Once solidified, the ceramic mold is broken away, revealing the metal casting. Any excess material or imperfections are then removed through various finishing processes, such as grinding or sandblasting, to achieve the desired final dimensions and surface quality.

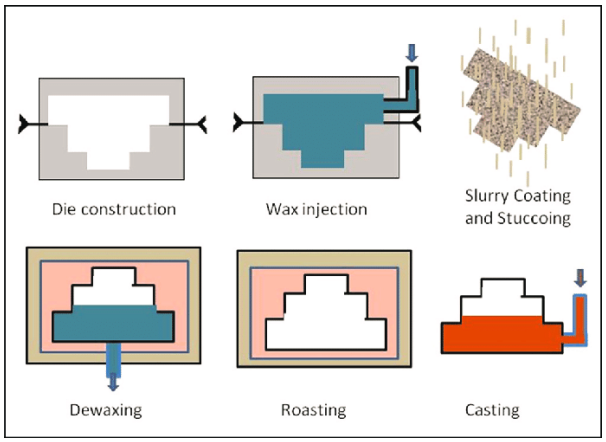

Figure 8: Investment casting process [14]

2.14. Dynamo

A dynamo is a device which simply converts the mechanical energy to electrical energy. the rotating shaft of the turbine is connected to the rotor of the dynamo. As the turbine rotates, it causes the rotor of the dynamo to rotate as well. Inside the dynamo, there is a stationary set of wire coils known as the stator and a rotating magnet (the rotor). As the rotor spins, it induces a current in the wire coils of the stator through electromagnetic induction. The DC output from the dynamo, now representing the electrical power generated by the turbine, can then be measured using appropriate instruments such as a multimeter or data acquisition system. This measurement allows you to monitor the power output of the turbine under various conditions. By using a dynamo in this setup, you can effectively measure the electrical output of the turbine, providing valuable information for performance evaluation, optimization, and monitoring purposes

Figure 9: Dynamo

CHAPTER THREE: METHODOLOGY

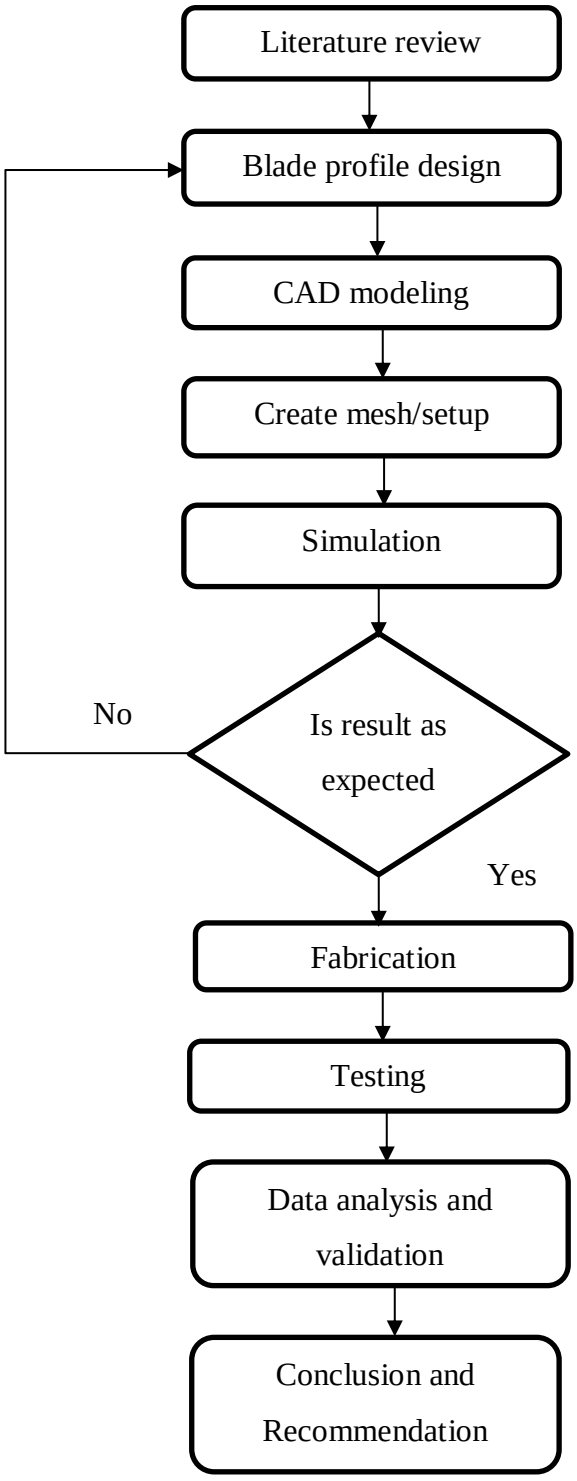

Figure 10: Project Flowchart

3.1. Modeling

In this initial phase, the blade profile of the Toroidal turbine is designed in CAD software like SolidWorks. Different blade profiles are designed for the comparative study of the effect of the change in the blade profile. Also, the key design parameters, such as blade shape, blade number, and rotor diameter are changed to form various iterations of the turbine.

3.2. Simulation

After the profile is designed, computational analysis is done multiple times on various models using ANSYS to find out the highest efficient model.

3.3. Fabrication

The optimal 3D design obtained after simulation in the CFD will be the basis for the fabrication. Material selection for the model will be chosen as per the market availability and with the comparison of the mechanical properties.

3.4. Experimental Setup and Testing

Experimentation will follow the design and fabrication of the blade profile. A pump is used to supply water to the turbine. The rotation of the turbine is captured by a shaft attached to the turbine. This shaft extends out of the pipe, and a gear is fitted onto it. The gear is then connected to a generator or dynamo. As the generator or dynamo rotates, it produces an electrical current and voltage, which can be measured using a multimeter.

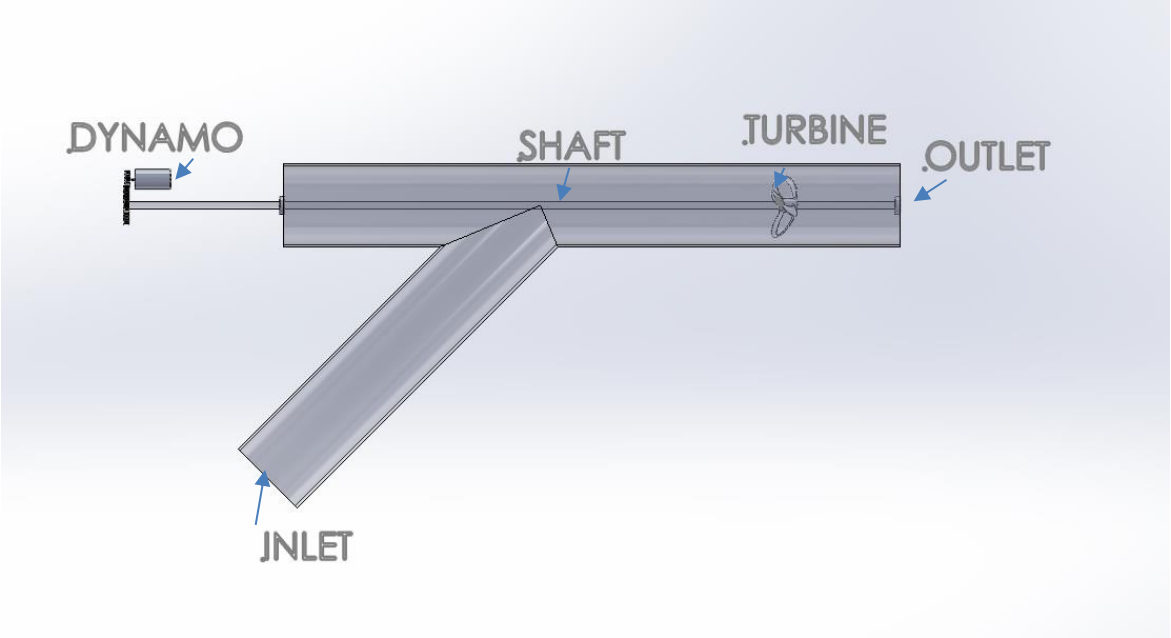

Figure 11: Turbine testing system

3.5. Documentation

The results obtained from CFD analysis and experimental setup will be documented regularly and properly.

CHAPTER FOUR: RESULTS AND DISCUSSION

4.1. Design of a toroidal turbine

4.1.1. Descriptive Geometrical Shape of Toroidal Profile

Based on the reference [11], toroidal propellers, where the blades form a closed intersecting structure with a cylindrical surface parallel to the hub of the propellor, result in two blade sections at the same radius 'r'. Which makes it challenging to express the geometric design parameters of toroidal propellers as a function of only radius. To smoothly represent the geometric shape of a toroidal profile, the concept of axial distance ’l’ is introduced. In addition, the toroidal profile also introduces parameters like outward lean angle, skew angle, and vertical angle. Axial distance 'l,' ranging from 0 to L, defines a curve serving as the reference line along the propeller's axial length. The equation and figure for the representation of the toroidal profile reference line are shown below.

$$x = l$$

$$r = r_l(l)$$

$$\theta = 0$$

In the equation, r_l represents the radius at axial distance 'l'.

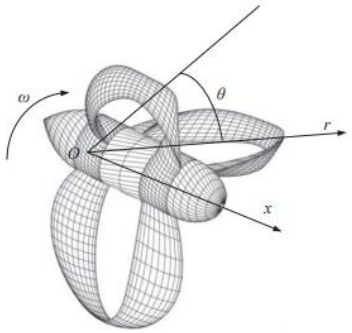

Figure 12: Definition of coordinate geometry of toroidal profile.[11]

The introduction of camber angle (φ) allows for adjusting the phase angle between front and rear sections. Typically, the front section has a negative camber angle, while the rear section adopts a positive angle, with the transition segment accommodating variations. Adding the effects of rake and camber angle to the reference line defines the blade's generator line. Hence, the generator line of the toroidal turbine blade can be

represented by the equation as shown below:

$$x = l + x_T(l)$$

$$r = r_l(l)$$

$$\theta = \varphi(l) + \theta_s(l)$$

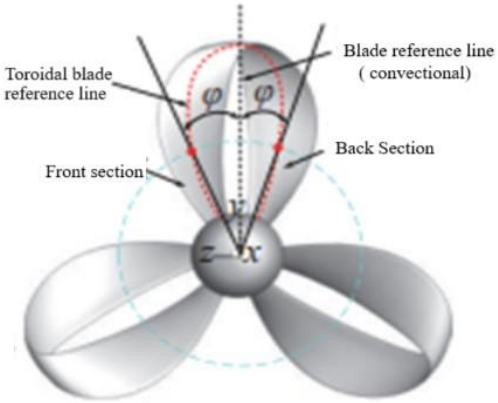

Figure 13: Blade reference line of a toroidal profile [11]

To better adjust the angle of attack of the blade section of the toroidal propeller and adapt it to the working environment, the introduction of the vertical angle (α) has been considered. The geometric meaning of the vertical angle is the angle between the chord line of the blade section and the tangent of rotation, as shown in Figure 14. Adjusting the vertical angle can either lift or pull the blade section relative to the tangent of rotation. Introducing the vertical angle in the transition section can allow the fluid to be drawn into the "ring" of the blade, but it also increases rotational resistance. Additionally, the vertical angle in the transition section can cause fluid to deviate from the incoming flow direction. Hence, it's crucial to reasonably adjust the vertical angle of the rotating blades.

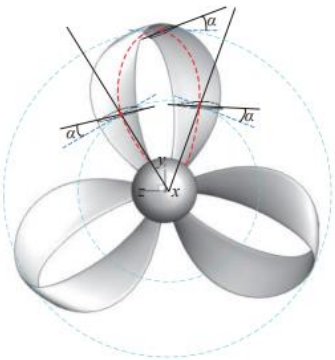

Figure 14:- Schematic diagram for a vertical angle for toroidal profile.[11]

Now the general equation of the cylindrical coordinates of a toroidal profile is given as:

$$x = l + x_T + \left[\left(-\frac{b}{2} + s\right) cos\,\alpha\right] sin\,\beta - \begin{bmatrix} y_b \\ y_f \end{bmatrix} cos\psi\, cos\beta$$

$$r = r_l - \left(-\frac{b}{2} + s\right) sin\,\alpha - \begin{bmatrix} y_b \\ y_f \end{bmatrix} sin\psi$$

$$\theta = \varphi + \theta_s + \frac{1}{r}\left\{\left[\left(\frac{-b}{2} + s\right) cos\,\alpha\right] cos\,\beta + \left[\begin{pmatrix} y_b \\ y_f \end{pmatrix} cos\,\psi\right] sin\,\beta\right\}$$

Where,

l= Axial distance ranging from 0 to L;

b = chord length of the blade section;

θs= skew angle;

ψ=rolling angle;

α= vertical rotational angle;

β = pitch angle;

φ= camber angle;

x_T= blade surface reference line;

s = chordwise distance from the point on the blade section to the trailing edge;

y_b = distances from points on the back of the blade section to the chord line and

y_f = distances from points on the face of the blade section to the chord line.

The three-dimensional coordinates of each cross-section at distance 'l' in the toroidal propeller within the Cartesian coordinate system o-xyz can be represented as:

$$x = l + x_T + \left[\left(-\frac{b}{2} + s\right) cos\,\alpha\right] sin\,\beta - \begin{bmatrix} y_b \\ y_f \end{bmatrix} cos\psi\, cos\beta$$

$$y = r cos\theta$$

$$z = r sin\theta$$

Now, to get the curve for two edges i.e., leading edge and trailing edge we modify the above expression. For both the leading edge and trailing edge, the value of 'y_b and y_h

is zero which reduces the above expression as: -

$$x = l + x_T + \left[\left(-\frac{b}{2} + s\right) cos\,\alpha\right] sin\,\beta$$

$$r = r_l - \left(-\frac{b}{2} + s\right) sin\,\alpha$$

$$\theta = \varphi + \theta_s + \frac{1}{r}\left[\left(-\frac{b}{2} + s\right) cos\,\alpha\right] cos\,\beta$$

For the leading edge, the value of s is zero, so the expression for the leading edge is as follows:

$$x = l + x_T - \frac{b}{2} cos\,\alpha\, sin\,\beta$$

$$r = r_l + \frac{b}{2} sin\,\alpha$$

$$\theta = \varphi + \theta_s - \frac{b}{2r} \cos\alpha\, cos\,\beta$$

For the trailing edge, the value of s is b, so the expression for the leading edge is as follows:

$$x = l + x_T + \frac{b}{2} cos\,\alpha\, sin\,\beta$$

$$r = r_l - \frac{b}{2} sin\,\alpha$$

$$\theta = \varphi + \theta_s + \frac{b}{2r} \cos\alpha\, cos\,\beta$$

In conclusion, the careful consideration of camber angles, rolling angles, and vertical angles plays a pivotal role in the design and optimization of toroidal turbines.

4.1.2. Design Calculation

For our study, we have the following parameters for the design of our turbine which are

a height of 1m and flow rate of 5m3/s. Applying the flow equation will give us outer and inner diameters. For the calculation of velocity, the energy equation is used. Knowing the value of velocity, flow rate, and the ratio of inner diameter to outer diameter we can easily calculate the diameter of the turbine.

Here,
Flow rate=5m3/s
Height=1m
Ratio of inner diameter to the outer diameter (Di/Do) =0.2

We know,

Potential energy = Kinetic energy

Or, mgh =1/2mv2

$V=\sqrt{gh} =\sqrt{} (2*9.81*1) =4.4294m/s$

Flow rate: $Q=A*V$

$Q=\pi/4 *(D_o^2-D_i^2) *V$

$4* 5=\pi (D_o^2-0.2D_o^{2)} *4.4294$

$D_o=1.224m$

Based on the established mathematical expression for toroidal propellers for leading edge and trailing edge, two curves are generated each representing the leading and trailing edge for the given geometric parameters of the toroidal propeller (such as total pitch, diameter, hub-to-diameter, chord length, pitch, rake, skew, sweep angle, lean angle).

Airfoils are the cross-sectional shapes of blades or foils that interact with the fluid flow, and their selection is paramount for achieving optimal efficiency and performance. The selection of airfoils was done considering various factors such as the ratio of lift to drag at required Reynold numbers, camber and thickness, and ease of manufacturing. For the geometry of a toroidal turbine, an airfoil with symmetry and a low angle of attack

is preferred. So, the NACA0015 airfoil is selected for the turbine geometry.

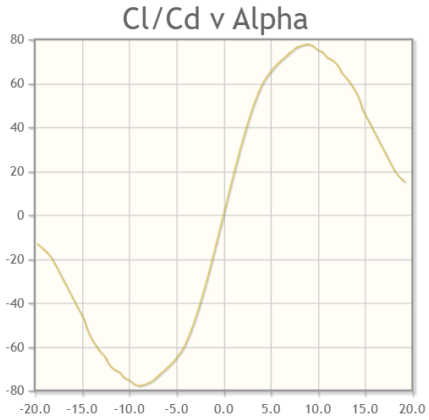

Figure 15:Cl/Cd vs alpha [7]

Table 2: Geometric features of the turbine

Length of turbine	244.8mm
The outer diameter of the turbine	1.224m
the ratio of hub/Outer diameter	0.2
number of blades	3
Airfoil	NACA0015

Using the values provided in tables 2 and 5 as input in the equation of leading edge and trailing edge we get the following coordinate for our leading and trailing edge. Plotting this coordinate gives us two spline curves for the leading edge and trailing edge as shown in figure 13.

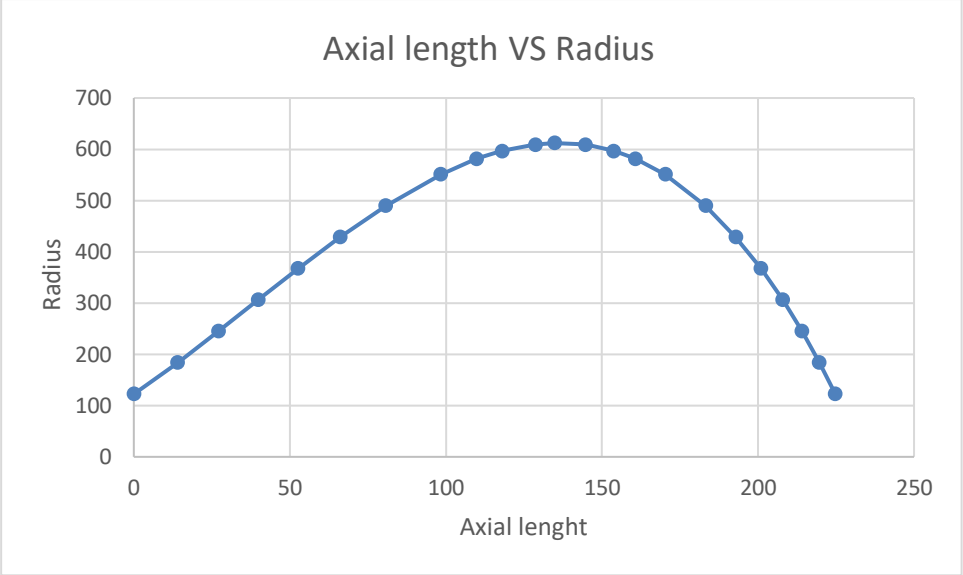

Figure 16: Axial Length vs Radius

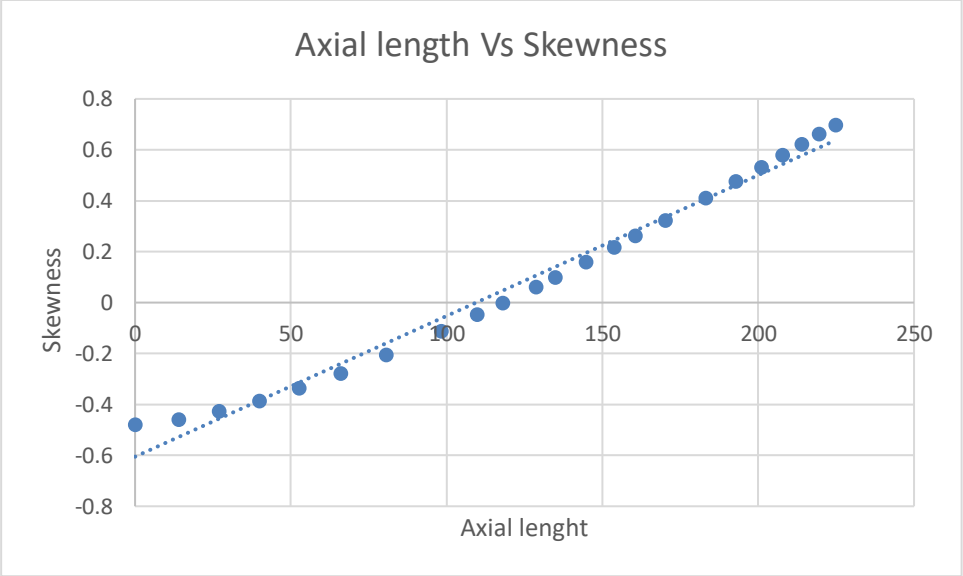

Figure 17: Axial length vs Skewness

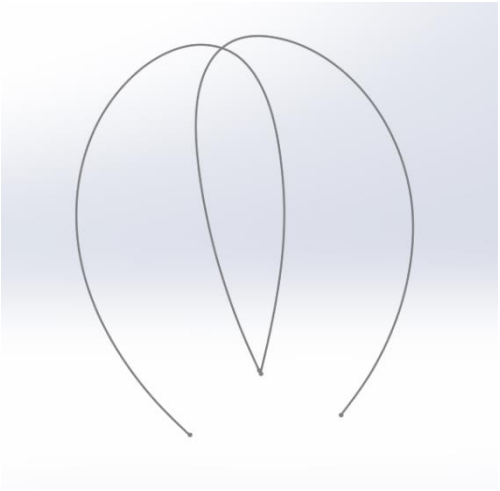

Figure 18: Guiding curves of leading and trailing edge

The three-dimensional model of the propellor is obtained after the integration of airfoil profiles between the leading and trailing edges. Using the loft feature in CAD software SolidWorks, the aerofoil geometry is lofted from the front section to the back using the above-obtained curves as guide curves. Adding a hub and circular pattern to make 3 no of blades gives us our required model. The obtained geometry of the toroidal propellor is shown in Figure 12:

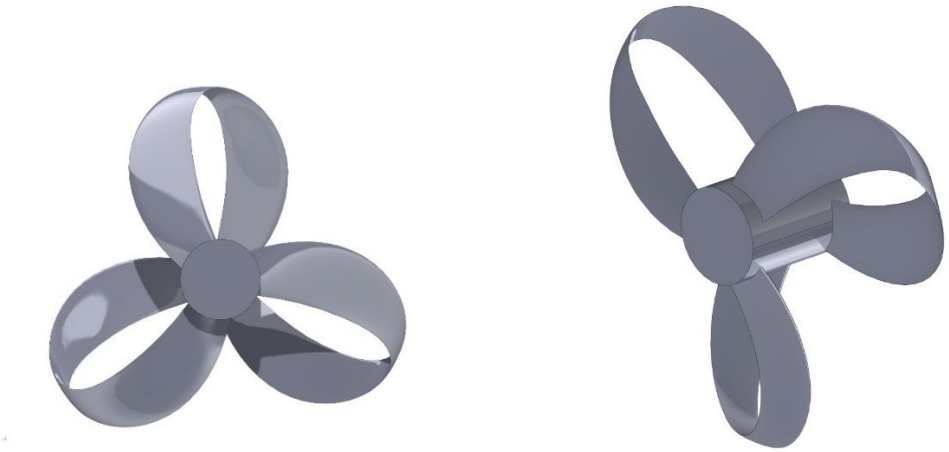

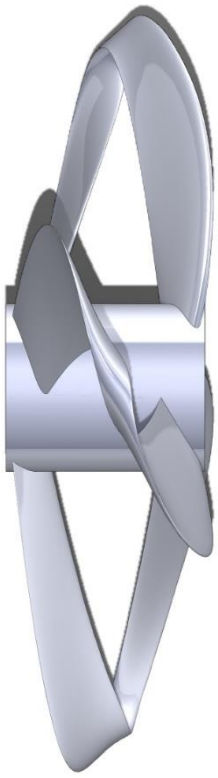

Figure 19: Various views of the CAD model

4.2. CFD Analysis

4.2.1. Fluid Flow Domain Formulation

For appropriate analysis, the overall domain was split into two sub-domains: surrounding fixed and inner rotating bladed domains. With the design modeler, the cylindrical fluid domain was created. Sufficient space before and after the turbine is provided to study the flow behavior. The Boolean was created to subtract the turbine from the cylindrical fluid domain. The boundary was named an inlet, outlet, walls, rotor, rotating domain, and stationary domain.

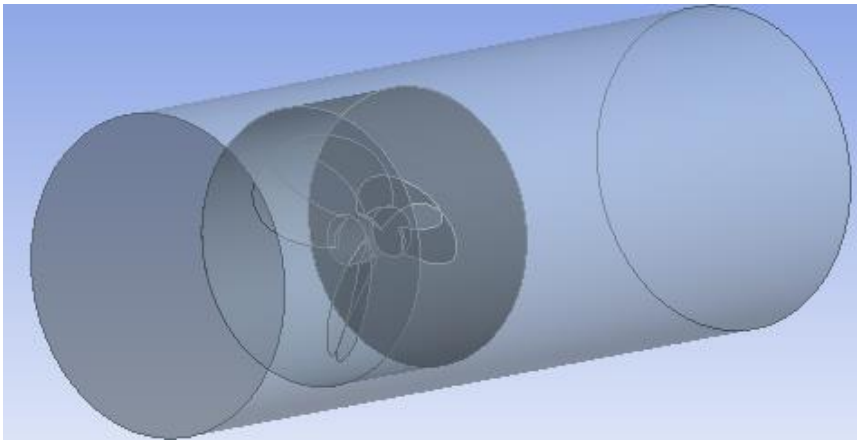

Figure 20: fluid flow domain

4.2.2. Meshing

To carry out the mesh generation of simulation, ANSYS Meshing is used. The mesh is generated in such a way that the size of cells near the blade wall is refined whereas, size increases towards the outer boundary. Also, the mesh of the rotating body is made smaller to capture the rotation of the turbine, and face sizing and edge sizing are used at the turbine surface and edge respectively. The inflation layer is utilized near the turbine surface to accurately capture the flow within the boundary layer thickness. In this model, 12 prism layers are used with a first layer height of 0.49 mm and a max growth rate of 1.20. The total count of elements is 2,088,070 and the number of nodes is 372,778 with minimum orthogonal quality of 0.20146 and maximum orthogonal quality of 0.99573 with average orthogonal quality of 0.76946 and standard deviation of 0.11933. The sectional representation of this obtained mesh is shown in the figure:

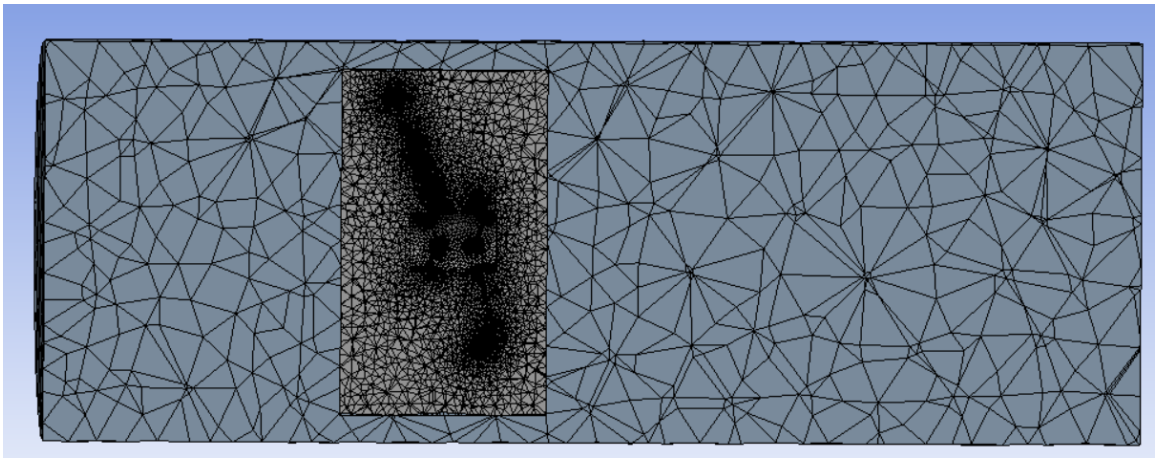

Figure 21: Meshing of the domain

4.2.3. Setup

The physics setup is done in ANSYS fluent and it involves defining fluid properties such as density and viscosity, selecting an appropriate turbulence model, and specifying boundary conditions, including those for rotating zones and wall conditions. For the turbulence model, k-omega SST is used as it is designed to provide accurate predictions for a wide range of turbulent flows, including attached and separated flows. The k-omega SST model combines elements of the k-epsilon and k-omega models to capture the advantages of both in different flow regions. Water is used as liquid and the properties of water are obtained via fluent database. Two domains are rotating and static domains. Mesh motion is implemented in a rotating domain with an angular velocity of 800 rpm along the X-axis. The boundary condition for the simulation includes an inlet velocity of 4.4254 m/s, a standard pressure outlet, and a no-slip turbine wall. After the setup is done, initiation is done and calculation is carried out.

4.3. CFD Results

After the simulation has been completed. Results were analyzed in CFD Post.

4.3.1. Pressure Contour

The pressure distribution on the turbine blade is analyzed. Since the turbine is a reaction-type turbine, energy conversion is due to a change in pressure. So, it is expected to have high pressure at the back and low pressure at the front, and due to the pressure difference between the front and back, a lift is generated and the turbine rotates. Figures 20 and 21 show the pressure distribution on the front and back sides of the turbine.

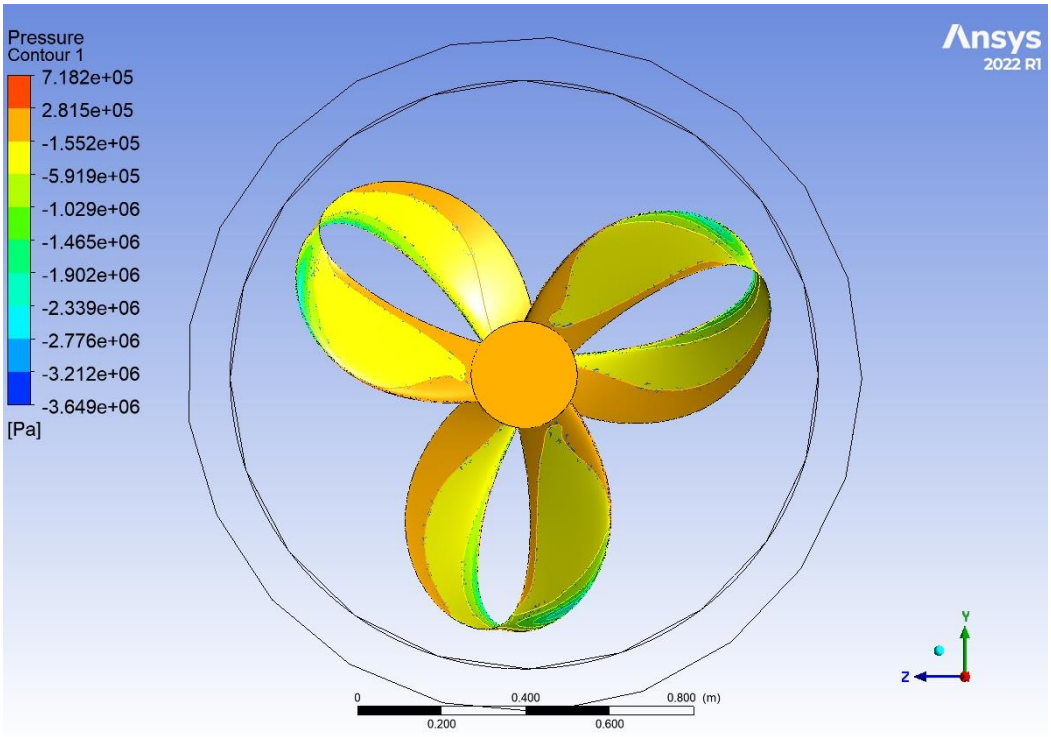

Figure 22: Pressure distribution on front of turbine blade

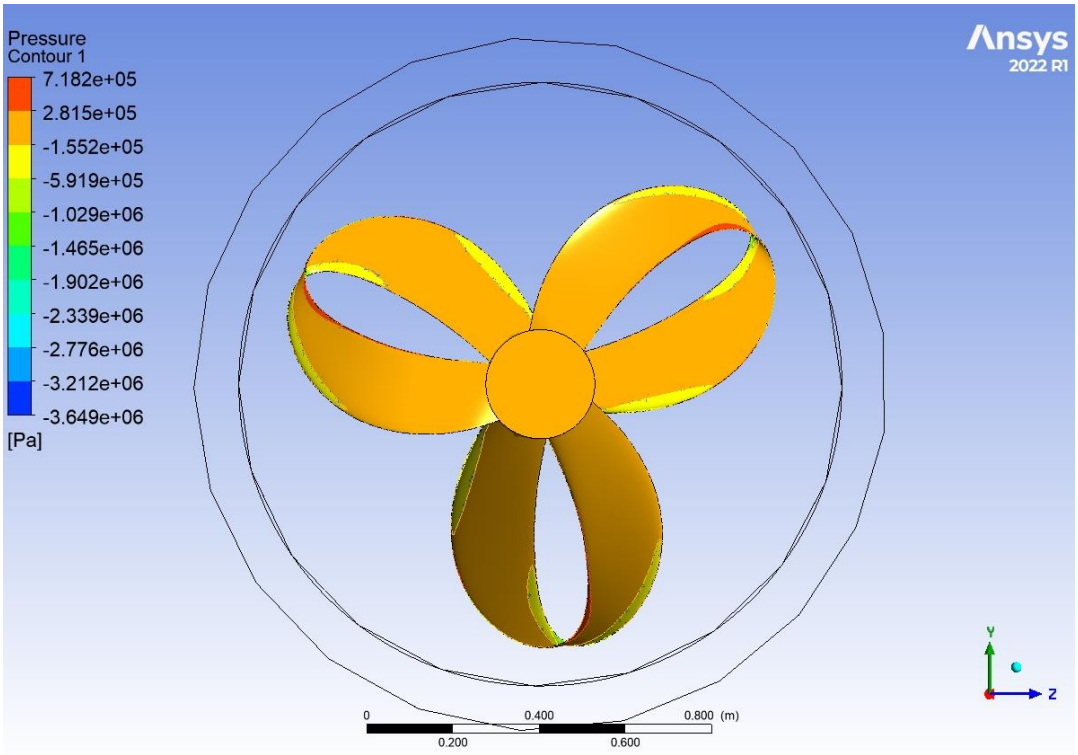

Figure 23: Pressure distribution on the back of the turbine blade

As indicated by the above figure, high pressure is at the back and low pressure is at the front which was expected, and due to this pressure difference between front and back, reaction turbine function.

4.3.2. Velocity Contour

Also, the velocity contour and its streamline are analyzed to understand the nature of the flow of fluid in the fluid domain. We already know that the energy conversion is due to pressure change so it is expected to have no velocity change at the inlet and outlet except near the wall and blade due to shear force and due to rotation of turbine and reduction of the area.

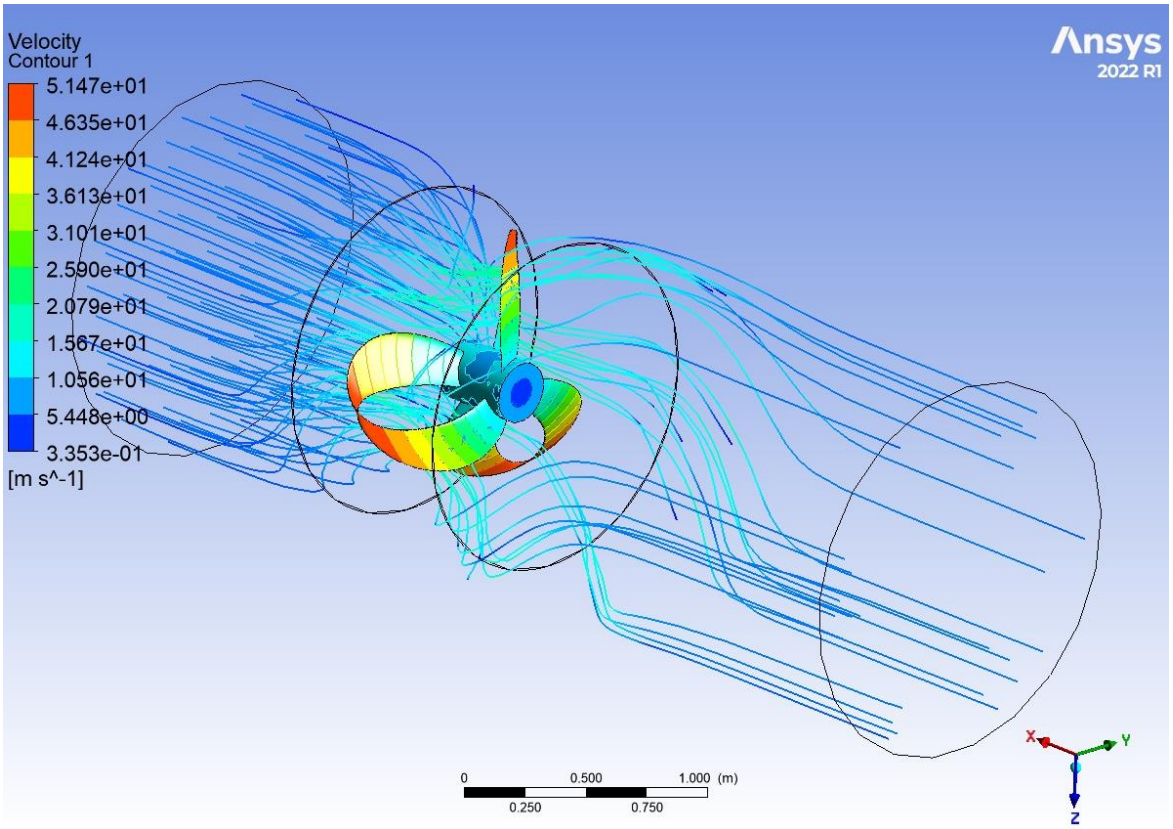

Figure 24: Velocity contour streamline across the fluid domain

4.3.3. Discussion and Conclusion

Also, the torque is calculated on the turbine blade wall and it is found to be 342.71 N.m. This torque is utilized to calculate the power generated and ultimately efficiency. Here, we have an operating rotation per minute (RPM) to be 800. So, the power calculated is

as follows:

Power(P) = Torque (τ) * Angular velocity (ω)

=342.71*2*π*800/60

=28710.8 watts

And energy available per second at the inlet is given as:

The energy available/sec (E) = ρgHQ

We have, density(ρ) = 997kg/m^3

Acceleration due to gravity (g) = 9.81 m/s^2

Head (H) = 1m

Flow rate(Q) = 5kg/m^3

So, E/sec= 997*9.81*1*5

=48,902.85 joules/sec

Now, the efficiency of the turbine is given as

$$\text{Efficiency}(\eta) = \frac{Power(P)}{Energy\ available(E/sec)} * 100\%$$

=28710.8/48,902.85*100%

=58.7%

Moreover, different parameters included during the design of the turbine influence heavily on turbine efficiency which needs to be studied further for the optimal design of the toroidal turbine.

4.4. Model Design

For our experiment, we have the following parameters for the design of our turbine which are flow rate and height of 1.4m given by the motor in the experimental setup. After measuring the height of the V-notch of angle 45°, we can calculate the flow rate.

Here,

Height of the V-notch=12.5cm

Angle of the notch=45°

Now,

$Q_t = \frac{8}{15}\sqrt{2g}\, H^{\frac{5}{2}} \tan\frac{\theta}{2}$

$Q_t = 5.405 * 10^{-3}\ m^3/sec$

Where Q_t is the theoretical discharge

Actual discharge (Q) = $C_d * Q_t$

$= 4.324 * 10^{-3}\ m^3/sec$

Where C_d is 0.78 to 0.85 for V-notch (0.8).

From the scaling laws: -

$$\frac{\mathbf{Q_p}}{\mathbf{Q_m}} = \left(\frac{\mathbf{H_p}}{\mathbf{H_m}}\right)^{1/2} \left(\frac{\mathbf{D_P}}{\mathbf{D_m}}\right)^{2}$$

On calculating with prototype and model test conditions. The scale ratio is found to be 9.415 and it was used to calculate the parameters of other components. Thus, our model diameter was found to be 132 mm.

4.5. Fabrication and testing

4.5.1. Y-shaped Pipe.

A Y-shaped pipe design is chosen to ensure water flows smoothly and efficiently through the pipe. This design also includes a passage for connecting a shaft to the turbine. The slanted part of the Y-pipe allows water to transfer smoothly from the main water supply to our turbine, while the vertical portion houses the shaft. Gravity helps guide the water downward, ensuring it hits the turbine and doesn't flow back out from the other side of the Y-pipe.

A liner metal pipe of a 6-inch diameter cast iron is cut into calculated length of 1.2

meters and 0.7 meters using the grinder. The initial step involves the formation of a Y connection, wherein two sections of the cast iron pipe, each of respective length, are joined together. This connection is welded to ensure structural integrity and then sealed using suitable sealing materials to prevent any leakage or ingress. Furthermore, to facilitate the integration of the pipe assembly into the water supply system, a flange is fixed to the Y piece. This flange serves as a robust interface point for connecting the assembled pipe to the main water channel, ensuring a reliable and leak-proof junction. Also, the gasket is added between two flanges to further tight seal the junction and restrict the leakage.

Figure 25:- Fabrication process of Y-pipe

4.5.2. Casting of turbine.

To begin the turbine fabrication process, the first step involves designing the turbine using SOLIDWORKS, based on the calculation already as mentioned. Once the turbine design is finalized, the next phase is generating an STL file from the SOLIDWORKS model. This file format, commonly used in 3D printing, serves as the blueprint for the physical fabrication process. During this stage, a thorough examination of the STL file is imperative to detect any anomalies such as surface imperfections or mesh irregularities that could hinder the subsequent printing process. Since the model of our turbine is small and the trailing edge has small features and also at the edge of the turbine there is a hard round shape and thin feature. So, careful consideration is provided in designing those parts and checking for the combability of 3D printing of the available machinery. With a validated STL file in hand, the turbine design is then translated into physical form through 3D printing technology. Utilizing specialized software, the STL file is imported and prepared for printing. PLA is used for the printing of our turbine, as it is cheaper and also fulfills our requirements.

To begin the investment casting process for turbine component fabrication, a silicone mold is created from the 3D-printed part, acting as a template for later stages. Next, a mixture of binder, refractory material, and water forms the investment casting slurry, which is spread over the silicone mold and left to dry into a sturdy shell. Once hardened, the shell is heated to remove the 3D-printed part, leaving a hollow cavity. Molten metal i.e., brass is then poured into the shell and allowed to cool, forming the turbine part. However, challenges like cracks in the shell or incomplete burnout of the 3D-printed part can affect the final product's quality, emphasizing the need for careful attention throughout the casting process. Upon successful completion of the casting process, the focus shifts towards post-processing and quality control measures. Inspection of the printed turbine parts for surface imperfections, dimensional accuracy, and structural integrity is conducted to identify any deficiencies. Subsequent post-processing steps, such as finishing, polishing, or heat treatment, are done to meet the desired specifications.

Figure 26:- Turbine Obtained After the Casting Process

4.5.3. Shaft Preparation.

A steel rod, approximately 1.8 meters in length, was processed on a lathe to create a machined shaft. The first step is to machine the stainless-steel rod in the lathe. The steel rod was secured in the lathe, and the machining process was initiated. The rod was carefully machined to a specific target diameter, ensuring a uniform and smooth surface throughout the shaft's length. Three distinct bearing spaces of internal diameter of 15mm were allocated along the length of the shaft. These bearing spaces were precisely machined to accommodate the necessary bearings that will support the shaft's rotation. The shaft also has a threaded area where the turbine will slip and it is fixed by using nuts. Careful attention to the shaft's diameter, bearing spaces, and surface finish ensures that the shaft will function reliably and effectively within the intended application.

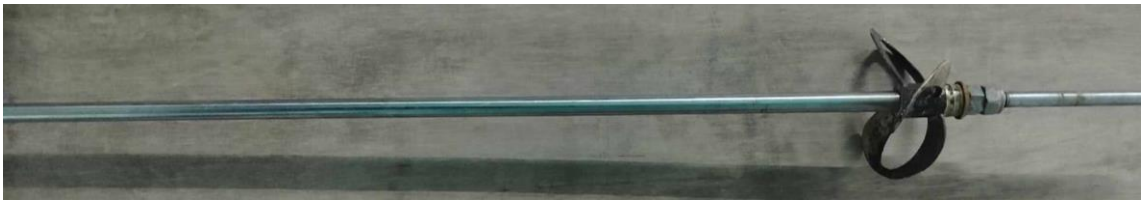

Figure 27:- Fabricated shaft

4.5.4. Gear Design

In the turbine testing setup, a pair of gears is utilized to transmit the rotational power from the turbine shaft to the dynamo, allowing for the generation of electrical energy. The turbine shaft is directly coupled to one of the gears, known as the driving gear. The second gear, referred to as the driven gear, is connected to the shaft of the dynamo. As the turbine shaft rotates, the driving gear also starts to spin which causes the dynamo shaft to rotate as well. For the designing of the gear CAD software SOLIDWORKS is used. This gear-to-gear coupling creates a mechanical linkage between the turbine shaft and the dynamo shaft. The gear ratio for the driver gear and driving gear is set to be 2:1. After the design is done, the model is converted into STL file which is then sliced using the slicer software of the respective 3D printer which is then 3D printed to obtain the required gears.

Figure 28 Gear system connecting shaft to dynamo

4.5.5. Testing

The turbine is tested using a closed-loop water supply system. A pump is used to supply water to the turbine, providing the necessary head (or pressure) to the system. This head increases the potential energy of the water, which is then converted into kinetic energy as the water flows through the pipe and strikes the turbine blades. The water is channeled through a closed pipe system to the turbine. As the water flows through the pipe, it strikes the turbine blades, causing a change in pressure. This change in pressure is what causes the turbine to rotate, converting the kinetic energy of the water into mechanical energy. The rotation of the turbine is captured by a shaft attached to the

turbine. This shaft extends out of the pipe, and a gear is fitted onto it. The gear is then connected to a generator or dynamo, which converts the mechanical energy from the rotating shaft into electrical energy. As the generator or dynamo rotates, it produces an electrical current and voltage, which can be measured using a multimeter.

By measuring the current and voltage, the electrical power generated by the system can be calculated. The efficiency of the turbine system can be calculated by comparing the electrical power generated to the input power provided by the pump. The input power can be determined by measuring the flow rate and head of the water supply. The ratio of the electrical power output to the input power provides the overall efficiency of the turbine system.

4.5.6. Result and Discussion

In the provided turbine testing scenario, a 12V dynamo is used to measure the electrical output of the turbine system. The rotational speed of the turbine is found to be 320 rev/mi. The electrical power output of the turbine is calculated using the formula:

Power = Current × Voltage Where:

- Current (I) = 0.9 Ampere
- Voltage (V) = 11.9 Volts

Electrical Power Output = I × V = 0.9 × 11.9 = 10.62 Watts

The input power to the turbine is determined by the change in the potential energy of the water flowing through the system. This change in potential energy is given by the formula:

Input Power = $\rho \times g \times H \times Q$

Input Power = 61 Watts

The efficiency of the turbine system is the ratio of the electrical power output to the input power, expressed as a percentage:

Efficiency = (Electrical Power Output / Input Power) × 100%

Efficiency = (10.62 Watts / 61 Watts) × 100% = 17.41%

This calculation provides the overall efficiency of the turbine system, taking into account the conversion of the water's potential energy into mechanical energy, and then the conversion of the mechanical energy into electrical energy through the dynamo.

4.6. Limitations

- A proper test rig for the toroidal turbine hasn't been defined yet. Different components like guide vanes, casing, draft tube, etc. in the case of the toroidal turbine need a detailed study. Thus, tests of toroidal profile as a turbine haven't been done so the test setup might not be suitable for this type of turbine.

- Further, in case of casting of turbine due to thin shape of the airfoil at the edges, casting is difficult so the shape was adjusted which can cause decrement in the turbine efficiency.

- The available resources, such as equipment, materials, and testing facilities, restrict the size and complexity of the turbine design.

- The testing setup and equipment may have inherent limitations, such as measurement accuracy, sensor precision, or the ability to replicate real-world operating conditions.

- Optimization of the various parameters have not been studied yet.

4.7. Problem faced

i. Due to the lack of a variable flow rate motor, experiments were limited to a single flow rate condition, restricting the exploration of the turbine's performance across various operating rates.

ii. The absence of a draft tube in the current setup led to water backflow, reducing the effective head and flow rate experienced by the turbine, ultimately impacting its measured performance.

iii. Compromises on the size, blade thickness, surface finish, and other specifications of turbine components and experimental apparatus had to be made due to the limited access to advanced machining and manufacturing instruments.

iv. Limited availability of the pipes and their fitting such as the diameter, material, and required for the turbine testing setup.

4.8. Work Schedule

The time for the project is shown in the Gantt chart below:

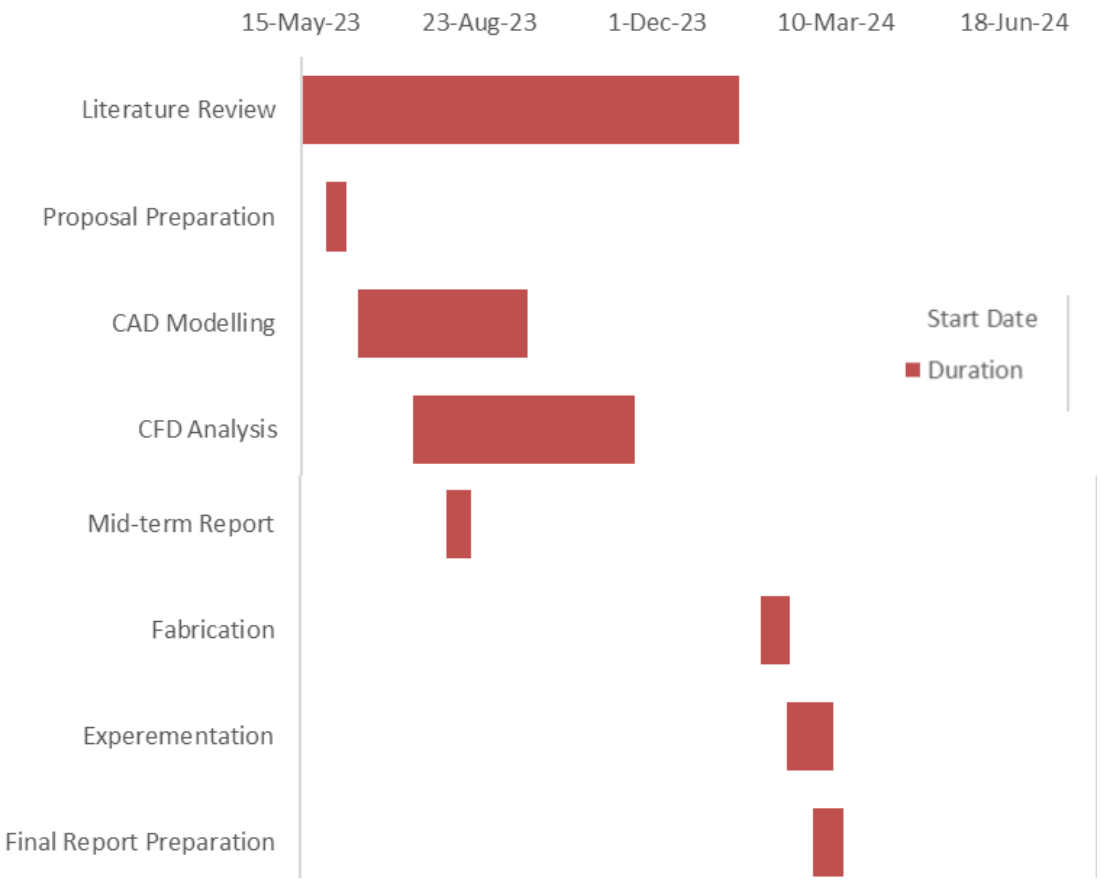

Figure 29: Gantt Chart

Table 3: Time Scheduling

Task	Start date	End date	Duration
Literature Review	15 May,2023	15 January,2024	8 months
Proposal Preparation	29 May,2023	8 June,2023	11 days
CAD Modelling	16 June,2023	18 September,2023	3 months
CFD Analysis	17 July, 2023	17 November,2023	4 months
Mid-term Report	15, December,2023	29 December,2023	14 days
Fabrication	29 January,2024	13 February,2024	15 days
Experimentation	13 February,2024	4 March,2024	21 days
Final Report Preparation	4th March,2024	7 April,2024	33 days

4.9. Cost Incurred

The cost of the overall project from start to finish is shown in the table below:

Table 4: Cost incurred

Particulars	Price (Rs.)
Documentation	3,000/-
Computational Cost	5,000/-
Bearing	1,000/-
Shaft	3,000/-
Casting	10,000/-
3D printing	2,500/-
Pipes and flanges	5,500/-
Human resource	5,000/-
Miscellaneous	5,000/-
Total	40,000/-

CHAPTER FIVE: CONCLUSION AND FUTURE ENHANCEMENT

5.1. Conclusion

In conclusion, the geometry of the toroidal turbine profile is developed using mathematical functions and various geometric parameters representing the geometry of the turbine. For the simulation of the turbine, ANSYS Fluent is utilized. For the head of 1m and $5m^3/s$ flow rate at 800 RPM, the efficiency is obtained to be 58.7%. For the experiment, a miniature model of the turbine is fabricated with a diameter of 132 mm on a scale of 9.415. The turbine is cast, and a custom experimental setup is constructed. Experiments were conducted on a flow rate of $4.324 * 10^{-3}$ m^3/sec and on a head of 1.4m. The rotational speed of the turbine is found to be 320 rev/min. The output data was obtained by measuring the electric output using a multimeter. The overall efficiency during the experimental setup is obtained to be 17.41%. While the current test results from the experimental setup may not fully represent the turbine's potential, the project has laid the groundwork for future development and optimization efforts.

5.2. Future Enhancement

To unlock the full potential of this turbine concept and pave the way for its practical applications in real-world energy systems, several avenues for future enhancement need to be explored. Some potential future enhancements are listed below: -

- A comprehensive study on the impact of factors like rated speed (RPM), turbine diameter, number of blades, and axial length can provide valuable insights to refine the turbine geometry and design.

- Study of the velocity triangle of the turbine to optimize the pitch angle, hydrofoil profile, and parametric curves. By optimizing these parameters, the turbine's performance can be further enhanced.

- Incorporating a draft tube in the setup can be done to minimize water backflow and ensure that the turbine experiences the desired head and flow rate.

- Explore opportunities for optimizing the experimental setup. By designing and constructing a specialized and optimal experimental rig, the true performance potential of the turbine can be accurately evaluated, yielding results that more closely align with the simulated predictions.

REFERENCES

[1] H. M. AUNG, N. A. SAN, and W. P. P. MYO, "Design and Performance Analysis of a Low Head Propeller Turbine," International Journal of Scientific Engineering and Technology Research, vol. 3, no. 9, pp. 1791–1795, May 2017. ISSN: 2319-8885

[2} R K Bansal, *A Textbook of Fluid Mechanics and Hydraulic Machines*. New Delhi: Laxmi Publications, 2010.

[3] "The British Hydropower Association A GUIDE TO UK MINI-HYDRO DEVELOPMENTS A Guide to UK mini-hydro development v3.0 A GUIDE TO UK MINI-HYDRO DEVELOPMENTS CONTENTS." [Online]. Available: www.british-hydro.org

[4] D. Zhou and Z. (Daniel) Deng, "Ultra-low-head hydroelectric technology: A review," *Renewable and Sustainable Energy Reviews*, vol. 78. Elsevier Ltd, pp. 23–30, 2017. doi: 10.1016/j.rser.2017.04.086.

[5] J. S. Carlton, Marine Propellers and Propulsion: John S. Carlton. Elsevier, Butterworth-Heinemann, 2012.

[6] K. M. Flood, "Propeller performance analysis using lifting line theory," thesis, Institute of Technology, Massachusetts, 2009

[7] Airfoil Tools, "NACA 0015 (ill. Cl=0.1)", airfoiltools.com. [Online]. Available: http://www.airfoiltools.com/airfoil/details?airfoil=naca0015-il. [Accessed: 13-Jan-2024].

[8] S. L. Dixon and C. A. Hall, *Fluid Mechanics and Thermodynamics of Turbomachinery*. Elsevier Butterworth-Heinemann, 2010.

[9] G. C. Sharrow, "Propeller," Mar. 13, 2017

[10] Y. Liyu, W. Chao, S. Cong, and G. Chunyu, “Mathematical expression method for geometric shape of a toroidal propeller,” *Chinese Journal of Ship Research*, vol. 19, no. 3, pp. 1–11, Aug. 2024. doi:10.19693/j.issn.1673-3185.03419

[11] S. Gaggero, J. Gonzalez-Adalid, and M. Perez Sobrino, “Design of contracted and tip loaded propellers by using boundary element methods and optimization algorithms,” *Applied Ocean Research*, vol. 55, pp. 102–129, 2016. doi:10.1016/j.apor.2015.12.004

[12] S. Z. BANG and L. Y. ZHONG, *Ships Principle*, vol. 2. Shanghai Jiaotong University Press, 2000.

[13] S. yu min and H. sheng, *Ship Propeller Theory*. Harbin Engineering University Press, 2003.

[14] C. Poli, "Metal Casting Processes," in Design for Manufacturing, C. Poli, Ed. Butterworth-Heinemann, 2001, pp. 115-126, ISBN: 9780750673419, doi: 10.1016/B978-075067341-9.50010-0.

[15] ANSYS, Inc., "Ansys Fluent Theory Guide," Release R2021 R2, Canonsburg, PA, July 2021.

[16] Wilcox, D. C., "Turbulence Modeling for CFD," 3rd Edition, DCW Industries, La Cañada, CA, 2006.

[17] R. K. Turton, *Principles of Turbomachinery*. London etc.: Chapman & Hall, 1995.

[18] B. Weigand and V. Simon, "Laws of Similarity in Fluid Mechanics," in Flow Phenomena in Nature, WIT Transactions on State of the Art in Science and Engineering, vol. 3, WIT Press, 2006, pp. 20-35.

APPENDIX

Table 5:-Geometric parameters of toroidal propellor

l/L	r_l/R	b/D	X_l/D	βº	θs°	φ°	α°
0	0.2	0.121	-0.062	15	0	-27.56	0
0.0624	0.3	0.1431	-0.0822	16	-0.89	-25.52	0.12
0.1203	0.4	0.16	-0.0933	17	-1.1	-23.44	0.62
0.1773	0.5	0.1723	-0.0968	18	-0.9	-21.26	1.44
0.2343	0.6	0.1797	-0.0928	19	-0.36	-18.93	2.61
0.2937	0.7	0.1806	-0.0807	20	0.43	-16.33	4.37
0.359	0.8	0.1683	-0.0587	21	1.46	-13.26	6.89
0.4377	0.9	0.1423	-0.0255	22	2.83	-9.33	9.39
0.4889	0.95	0.1228	-0.0022	23	3.78	-6.55	10.45
0.525	0.975	0.112	0.014	24	4.45	-4.56	10.98
0.5729	0.995	0.1027	0.0347	25	5.34	-1.86	11.41
0.6	1	0.101	0.0458	26	5.87	-0.24	11.51
0.6438	0.995	0.1065	0.0615	25	6.69	2.45	11.28
0.6842	0.975	0.119	0.0732	24	7.44	4.99	10.52
0.7146	0.95	0.1311	0.0789	23	7.99	6.95	8.97
0.7574	0.9	0.1514	0.0819	22	8.75	9.78	5.54
0.815	0.8	0.1763	0.0723	21	9.72	13.77	2.33
0.858	0.7	0.1869	0.0537	20	10.4	16.83	1.44
0.8941	0.6	0.1862	0.0298	19	10.94	19.44	0.98
0.9249	0.5	0.177	0.0024	18	11.39	21.74	0.63
0.9523	0.4	0.1626	-0.0272	17	11.77	23.82	0.38
0.9771	0.3	0.1447	-0.0584	16	12.11	25.74	0.17
1	0.2	0.124	-0.091	15	12.41	27.56	0

Table 6: Coordinate of leading-edge

X	Y	Z
-101.22	60.95	-106.14
-119.39	113.68	-144.25
-125.42	171.21	-175.11
-121.52	233.81	-197.62
-107.39	301.49	-209.93
-81.20	374.22	-209.10
-37.91	452.59	-187.93
26.30	533.97	-138.19
70.78	574.79	-93.69
100.89	594.78	-60.63
138.90	610.16	-17.04
158.20	613.65	7.61
185.49	609.85	41.82
205.93	596.04	66.96
217.14	579.33	82.00
225.64	546.92	96.82
221.12	484.07	104.89
206.75	422.69	100.86
187.59	362.04	91.27
165.14	302.07	77.64
140.37	242.94	59.95
113.62	184.49	38.41
86.26	125.94	12.55

Table 7: Coordinate of trailing edge

X	Y	Z
-50.56	121.93	10.70
-53.78	183.50	-3.40
-48.90	244.26	-14.66
-35.74	305.07	-21.95
-14.44	366.24	-23.88
15.70	427.68	-19.46
55.62	489.06	-8.96
108.07	549.85	14.49
143.64	579.20	37.64
169.42	592.70	58.12
203.62	600.72	90.42
223.68	599.99	111.74
254.52	587.65	150.42
280.88	563.10	187.86
297.29	536.29	214.76
315.37	486.55	248.13
322.29	397.58	275.85
310.46	318.48	277.24
287.35	248.02	262.36
256.57	185.41	235.99
221.20	129.26	201.47
182.72	78.53	160.58
140.57	32.10	113.80

Figure 30:- Reading of voltage on Multimeter

Figure 31:- Reading of RPM on Tachometer

Design and Fabricate a Toroidal Turbine for Low Head Hydropower Application

ORIGINALITY REPORT

22%
SIMILARITY INDEX

PRIMARY SOURCES

1	www.scribd.com Internet	123 words — 2%
2	Adhikari, Pradhumna, Umesh Budhathoki, Shiva Raj Timilsina, Saurav Manandhar, and Tri Ratna Bajracharya. "A Study on Developing Pico Propeller Turbine for Low Head Micro Hydropower Plants in Nepal", Journal of the Institute of Engineering, 2014. Crossref	66 words — 1%
3	mafiadoc.com Internet	61 words — 1%
4	da Silva, João Pedro Leite. "Computational Simulation of a Flow over the East Part of the Madeira Island", Universidade do Porto (Portugal), 2022 ProQuest	49 words — 1%
5	docplayer.net Internet	44 words — 1%
6	www.ijetae.com Internet	44 words — 1%
7	www.nitjsr.ac.in Internet	44 words — 1%